JOURNAL OF NATURAL PRODUCTS

Article

Cite This: J. Nat. Prod. XXXX, XXX, XXX−XXX

pubs.acs.org/jnp

# A Series of Enthalpically Optimized Docetaxel Analogues Exhibiting Enhanced Antitumor Activity and Water Solubility

Yun-Tao Ma,[†] Yanting Yang,[‡] Pei Cai,[†] De-Yang Sun,[†] Pedro A. Sánchez-Murcia,[§] Xiao-Ying Zhang,[†] Wen-Qiang Jia,[†] Lei Lei,[‡] Mengqi Guo,[‡] Federico Gago,[§] Hongbo Wang,*[,‡] and Wei-Shuo Fang*[,†]

[†]State Key Laboratory of Bioactive Substances and Functions of Natural Medicines, Institute of Materia Medica, Chinese Academy of Medical Sciences and Peking Union Medical College, Beijing 100050, People's Republic of China

[‡]Key Laboratory of Molecular Pharmacology and Drug Evaluation (Yantai University), Ministry of Education, Collaborative Innovation Center of Advanced Drug Delivery System and Biotech Drugs in Universities of Shandong, Yantai University, Yantai 264005, People's Republic of China

[§]Área de Farmacología, Departamento de Ciencias Biomédicas, Unidad Asociada al Instituto de Química Médica del CSIC, Universidad de Alcalá, E-28805 Alcalá de Henares, Madrid, Spain

Supporting Information

**ABSTRACT:** A dual-purpose strategy aimed at enhancing the binding affinity for microtubules and improving the water solubility of docetaxel led to the design and synthesis of a series of C-2- and C-3′-modified analogues. Both aims were realized when the C-3′ phenyl group present in docetaxel was replaced with a propargyl alcohol. The resulting compound, **3f**, was able to overcome drug resistance in cultured P-gp-overexpressing tumor cells and showed greater activity than docetaxel against drug-resistant A2780/AD ovarian cancer xenografts in mice. In addition, the considerably lower hydrophobicity of **3f** relative to both docetaxel and paclitaxel led to better aqueous solubility. A molecular model of tubulin-bound **3f** revealed novel hydrogen-bonding interactions between the propargyl alcohol and the polar environment provided by the side chains of Ser236, Glu27, and Arg320.

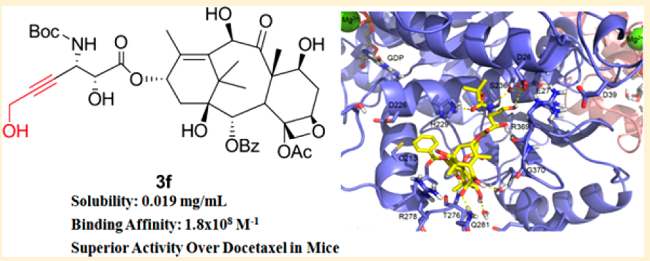


Cancer is the second leading cause of death globally, according to epidemiological data from WHO, and was responsible for 8.8 million deaths in 2015.[1] Numerous efforts on the development of targeted therapy have been made in the field of anticancer drug research in recent decades to fight this widespread disease. However, traditional cytotoxic drugs still play a very important role in cancer therapy. These agents can be used singly or combined as well as in combination with the so-called molecular-targeted antitumor agents. Such cytotoxic drugs include paclitaxel (**1a**, Figure 1) and its semisynthetic analogue docetaxel (**1b**, Figure 1), two tubulin-binding natural-product-derived molecules,[2] which have had documented great success in the treatment of ovarian, breast, lung, and various other cancers[3−5] since they were launched to market in the 1990s. Despite the widespread use of taxane-based antitubulin agents, both their compromised activity toward multidrug-resistant tumors and poor water solubility (causing formulation and pharmacokinetic problems) restrict their clinical uses.[6,7]

Investigations have revealed numerous antitumor drug-resistance mechanisms for taxane-based antitubulin drugs, of which three are important or clinically relevant:[8,9] (a) overexpression of ATP-dependent drug transporters, for example, P-glycoprotein (P-gp); (b) overexpression of tubulin isotypes with reduced drug-binding affinities, mainly $\beta$III tubulin; and (c) mutations in the taxane-binding site.

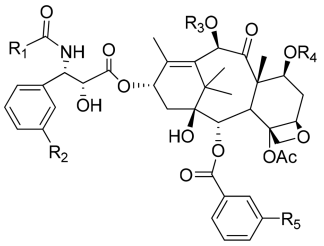

**1a** $R_1$=Ph, $R_2$=$R_4$=$R_5$=H, $R_3$=Ac
**1b** $R_1$=*t*-BuO, $R_2$=$R_3$=$R_4$=$R_5$=H
**1c** $R_1$=*t*-BuO, $R_2$=$R_5$=H, $R_3$=$R_4$=Me
**1d** $R_1$=*t*-BuO, $R_2$=$CH_2OH$, $R_3$=Ac, $R_4$=$R_5$=H
**1e** $R_1$=(*E*)-but-2-en-2-yl, $R_2$=$R_3$=H, $R_4$=propionyl, $R_5$=azido
**1f** $R_1$=*t*-BuO, $R_2$=$R_4$=H, $R_3$=propionyl, $R_5$=azido

**Figure 1.** Structures of paclitaxel (**1a**), docetaxel (**1b**), cabazitaxel (**1c**), CTX-63 (**1d**), LX-2-32C (**1e**), and Yg-3-46a (**1f**).

To overcome these drawbacks, modified taxanes with better antitumor activities and pharmacokinetic (PK) properties have been pursued.[10,11] However, none of them reached the market

**Special Issue:** Special Issue in Honor of Susan Horwitz

**Received:** October 10, 2017





DOI: 10.1021/acs.jnatprod.7b00857
J. Nat. Prod. XXXX, XXX, XXX−XXX

**Scheme 1. Synthesis of Taxanes 2a−2g**

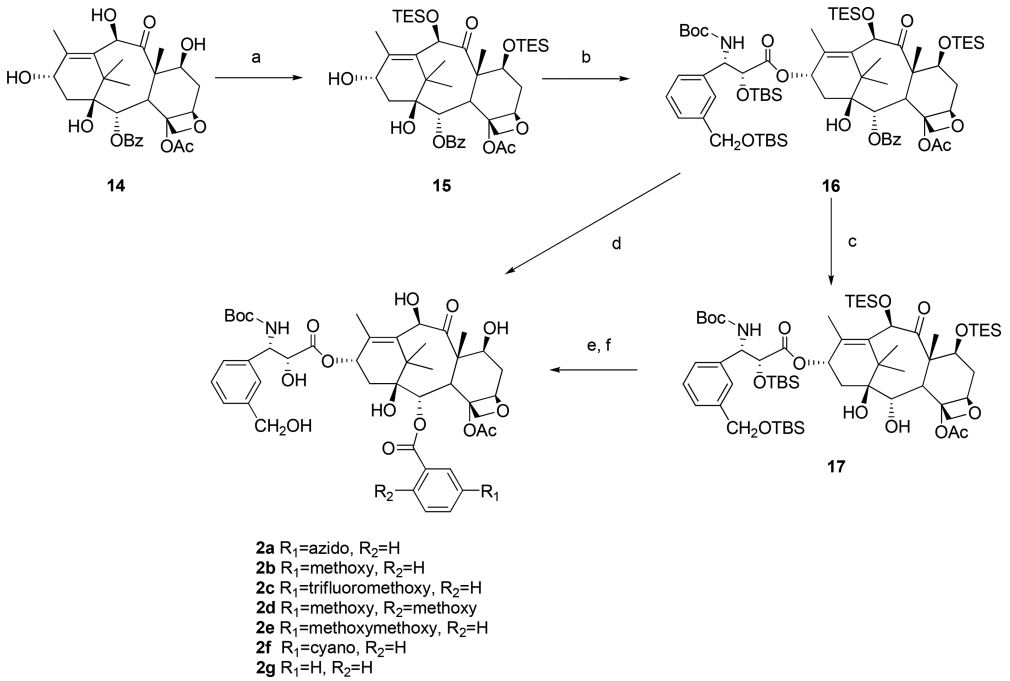


**Table 1. Microtubule Binding Constants and Cytotoxicities of Taxanes 2 and Reference Drugs**

| | | IC$_{50}$ (nM) | | | | | |
|---|---|---|---|---|---|---|---|
| compound | $K_b$ 35 °C ($M^{-1}$) | A2780 | A2780AD[a] | R/S[b] | HeLa | HeLa/βIII[c] | R/S[d] |
| paclitaxel (**1a**) | $3.3 \times 10^6$ | 13.4 | 16040 | 1197 | 4.6 | 41.0 | 8.9 |
| docetaxel (**1b**) | $2.1 \times 10^7$ | 11.2 | 21650 | 1933 | 3.5 | 27.1 | 7.7 |
| **2a** | $6.1 \times 10^8$ | 2.6 | 1171 | 450 | 1.6 | 9.4 | 5.9 |
| **2b** | $2.4 \times 10^7$ | 28.6 | 144.0 | 5.0 | 2.9 | 38.8 | 13.4 |
| **2c** | $2.8 \times 10^7$ | 21.3 | 1750 | 82 | 4.2 | 43.2 | 10.3 |
| **2d** | $2.7 \times 10^7$ | 21.6 | 376.0 | 17 | 4.3 | 47.5 | 11.0 |
| **2e** | $6.1 \times 10^6$ | 31.9 | 1947 | 61 | 7.5 | 108.0 | 14.4 |
| **2f** | $6.4 \times 10^6$ | 153.0 | 7561 | 49 | 45.4 | 461.0 | 10.2 |
| **2g** | $4.7 \times 10^6$ | 30.8 | 2227 | 72 | 21.7 | 242.0 | 11.0 |

[a]Resistant ovarian carcinoma cells overexpressing P-gp. [b]The relative resistance values were calculated by dividing the IC$_{50}$ value of the resistant ovarian carcinoma cells by the IC$_{50}$ value of the nonresistant ovarian carcinoma cells. [c]βIII transfected human cervical carcinoma cells HeLa cell line (wild-type βIII). [d]The relative resistance values were calculated by dividing the IC$_{50}$ value of the βIII transfected cell line (wild-type βIII) by the IC$_{50}$ value of the parental HeLa cell line.

until cabazitaxel (**1c**, Figure 1), a poor substrate of P-gp that remains active in docetaxel-resistant tumors,[12] was approved by the U.S. FDA in 2010 for the treatment of metastatic refractory prostate cancer.[13]

In the earlier study,[14] it was found that enhancing the microtubule (MT) binding affinity of taxanes could be utilized to combat drug-resistant tumors overexpressing P-gp. This new strategy was also confirmed in subsequent research leading to CTX-63 (**1d**, Figure 1), a reported C-3′-modified docetaxel analogue that was successfully predicted as a tighter MT-binding molecule in the comparative binding energy (COMBINE) analysis. The higher affinity of **1d** for β-tubulin resulted from a more favorable interaction between the benzylic hydroxy group at C-3′ and the side chain of Glu27 in the paclitaxel-binding site.[15]

Previously, two paclitaxel analogues, LX-2-32C (**1e**, Figure 1)[14,16] and Yg-3-46a (**1f**, Figure 1),[17,18] were selected as candidates for antitumor drug development, both of which are more potent than paclitaxel in drug-resistant tumors and also equally or more hydrophobic than this reference taxane. As it has been recognized that the "molecular obesity"[19,20] during the lead optimization process may result in poor PK properties, the discovery of **1d** through setting up a new water-shielded hydrogen bond between a hydroxy group in the ligand and tubulin, i.e., an enthalpy-driven process, could be valuable in finding new drug candidates with better PK and also improved water solubility.

In this study, further optimization of **1d** was effected by modifications at C-2 and/or C-3′ of this taxane, as both positions were known to greatly impact taxane−tubulin interactions and also cytotoxic activity.[11,17,21,22] It was hoped to optimize the semisynthetic taxanes through an enthalpically driven process, thus retaining and/or improving pharmacodynamics (PD) together with PK properties. As a result of these efforts, a C-3′-modified docetaxel analogue, **3f**, was found that exhibits more potent antitumor activity than docetaxel in vivo.


DOI: 10.1021/acs.jnatprod.7b00857
J. Nat. Prod. XXXX, XXX, XXX−XXX

## RESULTS AND DISCUSSION

**C-2-Modified Docetaxel Analogues.** C-2 substitutions are known to be critical for the taxane−MT binding affinity.[17] Several optimal substituents were chosen from literature data[23,24] to replace the 2-benzoate in CTX-63 (**1d**). The synthesis of the C-2-modified CTX-63 was similar to that in a previous study,[15] but was optimized by replacement of a 2′-*O*-silyl protective group to improve the overall yield. Coupling of the protected baccatin III **15** and the corresponding *β*-lactam (Scheme S1, Supporting Information) furnished the intermediate taxane **16** bearing a C-3′ *m*-TBS-*O*-hydroxymethylphenyl group, which was subjected to hydrolysis, esterification, and deprotection, successively. More specifically, treatment of **16** with anhydrous potassium hydroxide afforded the C-2 debenzoyl intermediate **17** in 41% yield based on 44% of substrate **16** recovery. Taxanes **2a**−**2f** were afforded via the esterification of 2-debenzoyl intermediate **17** with various substituted benzoic acids in the presence of dicyclohexylcarbodiimide (DCC) and 4-dimethylaminopyridine (DMAP), followed by desilyation, while **2g** was obtained by the deprotection of **16** (Scheme 1). It is worth mentioning that the *tert*-butyldimethylsilyl (TBS) group was chosen to replace a triethylsilyl (TES) group in the previous report,[15] as the TES group was removed during the C-2 esterification step, and C-2 and C-2′ diesterified products were obtained almost exclusively.

C-2 derivatives of **1d** were then tested in both molecular and cellular assays (Table 1). The highest MT binding affinity derivative **2a** found was the 2-*m*-azido-substituted compound, as in most taxane studies. Compound **2a** was also the most cytotoxic compound in two pairs of drug-sensitive and -resistant (P-gp and *β*-III tubulin overexpression mechanisms) tumor cells among the series **2a**−**2g**, with a 29-fold enhancement in MT binding affinity, and was 4−5 times more cytotoxic against A2780 drug-sensitive cells and 18−19 times more active against A2780AD-resistant cells (P-gp overexpressed). This, again, demonstrated the utility of the proposed strategy.[14,17] None of the derivatives other than **2a** was better than the reference compounds **1a** and **1b** for both HeLa and *β*-III transfected drug-resistant HeLa/*β*III cells. However, **2a** did not exhibit superior activity to docetaxel in A2780 and A2780AD xenografted mice. This fact significantly reduces the possibility of progressing the C-2-modified CTX-63 as a new drug candidate.

**C-3′-Modified Docetaxel Analogues.** Next, C-3′ of **1d** was explored through the introduction of various hydrogen bond (HB) donors and acceptors, as well as introducing negatively and positively charged groups, into this position. The rigidity of the linker (phenyl ring) between C-3′ and the terminal functional group (hydroxy) was explored by replacing the phenyl with alkynyl, alkenyl, and alkanyl moieties.

In general, the corresponding *β*-lactams were first synthesized and then coupled to protected baccatin III, while during the preparation of **3a**−**3d** functional group interconversion was applied, thereby converting **22** (protected **1d**) into **3a**−**3d**.

A routine *β*-lactam synthetic route[15] furnished **20**, in which the OH groups were protected by TBS and TES. The *β*-lactam **20** was coupled to 7,10-*O*-di(triethylsilyl)-10-deacetylbaccatin III (DAB) (**15**) to obtain **21**. Selectively removing the TES protective group on benzyl alcohol by HF/pyridine (Py) in an ice bath afforded the intermediate **22**, which was then converted to taxanes **3a**−**3d** under various conditions (Scheme 2). Treatment of **22** with pyridinium dichromate (PDC) and

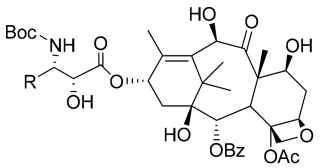


**3a** R=3-formylphenyl
**3b** R=3-(methoxymethyl)phenyl
**3c** R=3-carboxyphenyl
**3d** R=3-((dimethylamino)methyl)phenyl
**3e** R=3-(2-hydroxyethyl)phenyl
**3f** R=3-hydroxyprop-1-ynyl
**3g** R=(*Z*)-3-hydroxyprop-1-enyl
**3h** R=(*E*)-3-hydroxyprop-1-enyl
**3i** R=3-hydroxypropyl

**Figure 2.** Structures of the C-3′-modified CTX-63 analogues **3a**−**3i**.

deprotection formed aldehyde **3a**. Taxane **3b** was obtained by methylation in the presence of di-*tert*-butyl-4-methylpyridine (DTBMP) and methyl iodide and deprotection. *N*-Methylmorpholine-*N*-oxide (NMO) oxidation of **22** catalyzed with tetrapropylammonium perruthenate (TPAP) furnished a *m*-formyloxy-substituted compound, which was deprotected to afford **3c**. Finally, **3d** was synthesized by following a three-step procedure, namely, attachment of a leaving *O*-tosyl (OTs) group onto the *m*-OH on C-3′ phenyl, nucleophilic replacement of OTs with dimethylamine, and deprotection.

The *β*-lactam **35a** bearing a C-3′ *m*-(2-hydroxyethyl)phenyl substitution was synthesized following a route similar to that leading to *β*-lactam **13** (Scheme 3). Treatment of 2-(3-bromophenyl)ethanol **23** with *n*-butyllithium and dimethylformamide (DMF) afforded aldehyde **24**, which was then protected by a TBS group. A Staudinger reaction was applied to the adduct formation of imine **30a** and ketene prepared from acetoxyacetyl chloride to furnish racemic *β*-lactam **31a**. During removal of the *p*-methoxylphenyl (PMP) group by ceric ammonium nitrate (CAN) oxidation, TBS was also removed to afford racemic lactam **32a**. After kinetic resolution of racemate **32a**, protective groups were reintroduced to the lactam **33a**, affording *β*-lactam **35a** over three steps. Coupling of 7,10-*O*-di(triethylsilyl)-10-DAB (**15**) with *β*-lactam followed by deprotection afforded **3e** with one more carbon having *meta*-substitution on the C-3′ phenyl. The extension of the *meta*-alkyl chain on phenyl aimed to optimize the interaction of the ligand with the surroundings of Glu 27 in *β*-tubulin, as revealed in the previously reported COMBINE model.[15]

Further optimization of C-3′ substituents was performed by replacing the phenyl with alkynyl, alkenyl, and alkanyl moieties.

The alkynyl-substituted *β*-lactam **35b** was synthesized from 2-butyne-1,4-diol (**26**) as the starting material (Scheme 3). Selective monohydroxyl protection of **26** followed by oxidation afforded **25b**, which was transformed into imine **30b** and then formed *β*-lactam adduct **31b**. After several steps of transformation including resolution, chiral *β*-lactam **35b** was obtained and coupled with 7,10-*O*-di(triethylsilyl)-10-DAB (**15**) followed by deprotection to afford taxane **3f**. Upon hydrogenation of **3f** with Lindar's catalyst or Pd/C, *cis*-alkenyl-bearing **3g** and alkanyl **3i** were obtained.

However, the *trans*-alkenyl analogue **3h** could not be obtained directly by reduction of **3f**, so *β*-lactam **35c** was synthesized alternatively, that is, starting from (*E*)-but-2-ene-1,4-diol **28** (Scheme 3) and following a procedure similar to that leading to the synthesis of *β*-lactam **35b**. Coupling of **35c** with 7,10-*O*-di(triethylsilyl)-10-DAB (**15**) followed by deprotections afforded **3h**.


DOI: 10.1021/acs.jnatprod.7b00857
J. Nat. Prod. XXXX, XXX, XXX−XXX

**Scheme 2. Synthesis of Taxanes 3a−3d**

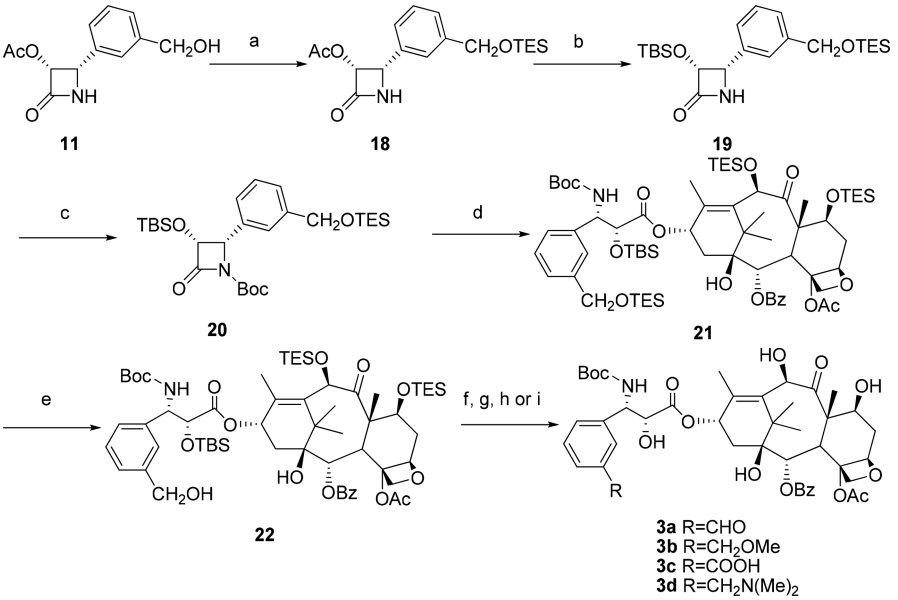


Among the C-3′-modified taxanes obtained, only **3f** and **3h** showed higher binding affinities for tubulin relative to that of docetaxel, with **3f** bearing a 3′-(3-hydroxylprop-1-ynyl) group being endowed with ca. 8 times higher affinity. The extension of one carbon into *m*-hydroxymethylphenyl or the replacement of the phenyl with a *cis*-/*trans*-ethylene or an ethyl group resulted in as much as a 500-fold reduced binding affinity. Interestingly, C-3′-modified taxanes bearing hydroxyformyl (**3c**) and dimethylamino (**3d**) groups showed diminished binding affinities.

The propargyl alcohol present in taxane **3f** is directed, as reported for the benzyl alcohol of CTX-63,[15] toward the hydroxy group of Ser236 and the carboxylate of Glu27, which is held in place by the guanidinium groups of Arg243 and Arg320 (Figure 3). During the molecular dynamics simulation, additional long-lived hydrogen bonds are established between the oxetane oxygen and the NH of Thr276, the carbonyl O-9 and the side-chain carboxamide of Gln281, the C-3′ benzamide carbonyl oxygen and $N^{\varepsilon}$ of His229, the hydroxy O-2′ and the backbone carbonyl of Arg369, and, through an intervening long-residence water molecule, between N-3′ and the carboxylate of Asp27. In this respect, it was noted that the impact on binding affinity of the first hydration shell of protein−ligand complexes is often overlooked, in agreement with other authors.[25] It is believed that the polar environment surrounding the propargyl alcohol in the bound conformation enthalpically boosts the binding energy relative to docetaxel (**1b**), which has an unsubstituted phenyl ring in this position. In fact, when calculating the binding energies and component contributions for the association of **3f** and docetaxel with *β*-tubulin at the interprotofilament site (Table 2), similar values within experimental error were obtained. According to these data, this similarity is most likely due to the fact that the intended gain in binding enthalpy was obtained through improved electrostatic interactions and a lower penalty for receptor desolvation but at the cost of a loss of van der Waal's interactions, because of the replacement of the bulky phenyl ring with the linear alkynyl group. In fact, similar binding signatures were obtained when pairwise comparing the solvent-corrected residue-based contributions for these two molecules (Figure 4). This proposed binding mode also accounts for the importance of the spatial position of the hydroxy group in taxanes **3g−3i**, as the *E*-configuration taxane **3h** displayed ca. 146 times higher binding affinity than the *Z*-configuration taxane **3g**. The lower binding affinity for taxane **3i** relative to **3f** could be explained by the much larger flexibility of its side chain, leading to decreased enthalpic contributions and a higher entropic penalty.

Next, the cytotoxicities in two pairs of drug-sensitive and drug-resistant tumor cell lines were assessed (Table 3). The highest binding-affinity taxane **3f** was the most active in the C-3′-modified series **3**, but still less active than paclitaxel (**1a**) and docetaxel (**1b**) in both sensitive and resistant tumor cell lines, while the resistant indices were improved slightly. Compared with **2g** (the 10-deacetyl derivative of CTX-63), both functional group replacements (**3a** and **3b**) and prolonged linkage (**3e**) decreased the cytotoxicity 1.3- to 109-fold, and introduction of charged groups (**3c** and **3d**) resulted in complete activity loss. Taxanes **3a** and **3h** were similar to or a little less active than **3f** against the two cell lines, and **3g** and **3i** were much less active.

As the high binding-affinity taxane **3f** displayed potent cytotoxicity against both drug-sensitive tumor cells and drug-resistant tumor cells, it was selected for animal model evaluation. In drug-sensitive ovarian cancer A2780 xenografted mice, **3f** showed similar inhibitory effects at different doses (10 and 20 mg/kg) to that of paclitaxel (20 mg/kg) (Table S1, Supporting Information) and demonstrated superior activity to docetaxel in mice bearing drug-resistant ovarian cancer A2780/AD xenografts in a dose-dependent manner (Table S2, Supporting Information) (Figure 5).

To facilitate the better understanding of pharmacodynamics for **3f**, its pharmacokinetics was also analyzed as shown in Figure 6 and Table S3, Supporting Information. The plasma drug concentration observed was higher in the **3f** liposome group than that in the docetaxel group at 12, 24, 48, 72, and 96 h postadministration, and the accumulation and clearance of docetaxel (**1b**) occurred over a considerably shorter period when compared with the **3f** liposome group.

**Water Solubility Evaluations.** The initial design for these CTX-63 analogues also aimed to enhance the water solubility of



DOI: 10.1021/acs.jnatprod.7b00857
J. Nat. Prod. XXXX, XXX, XXX−XXX

**Scheme 3. Synthesis of Taxanes 3e−3i**

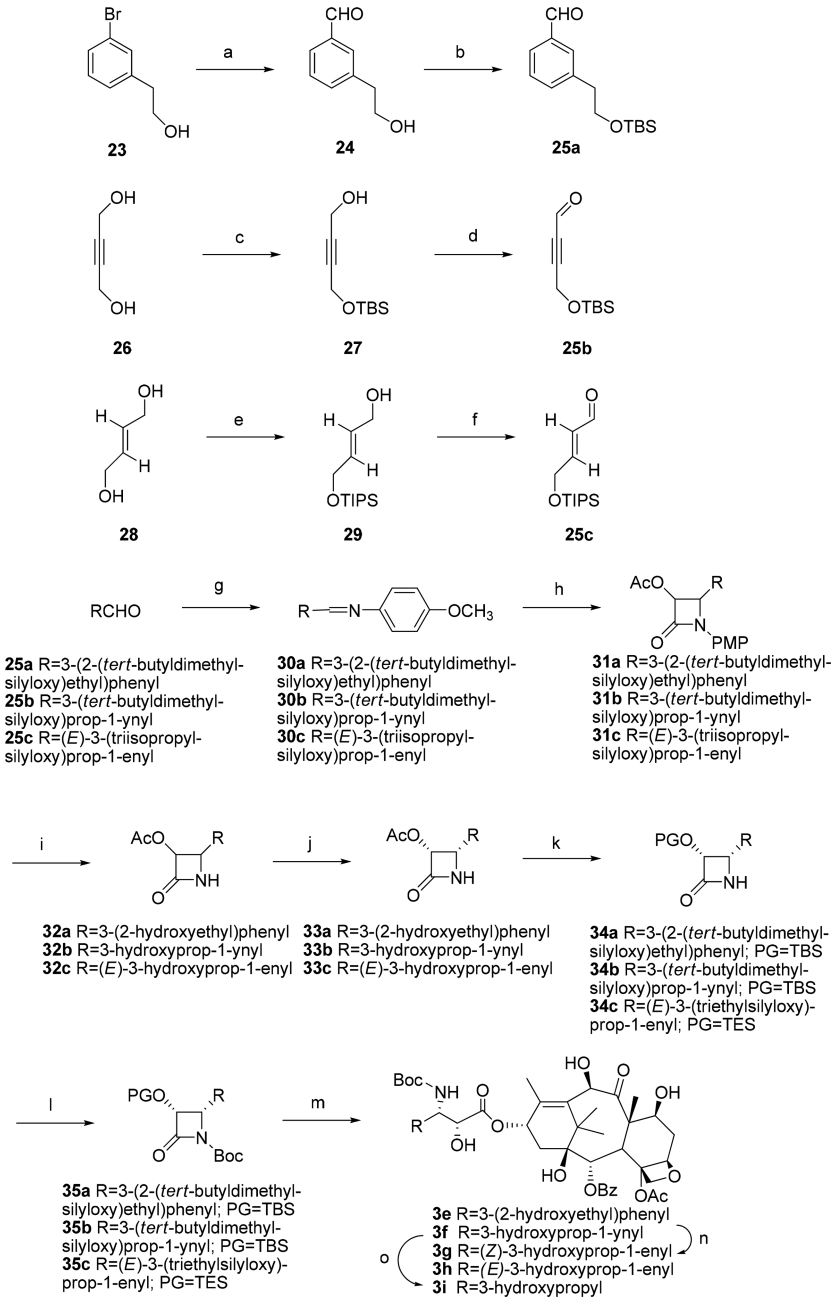


hydrophobic taxanes so as to improve the PK properties as well as facilitate its formulation. Following a reported procedure,[27] the water solubility of the synthesized compounds **2** and **3** was measured by reversed-phase HPLC (Table 4). All compounds showed improved water solubility compared to docetaxel and paclitaxel (31−135 times), among which the most potent taxane, **3f**, was found to be about 3-fold more water soluble than docetaxel.

As it is known that high-affinity taxanes may overcome P-gp overexpression-mediated tumor drug resistance,[17] semisynthetic taxanes [e.g., Lx-2-32c (**1e**),[14,16] Yg-3-46a (**1f**)[18]] with such properties at the molecular level were prepared. Although potent cytotoxicity especially against drug-resistant cells was well established, such highly hydrophobic molecules did encounter some problems (e.g., unfavorable PK and difficulty in formulation) in their evaluation.

It was reasoned that such problems are due, at least in part, to the hydrophobic nature of these semisynthetic taxanes, which were obtained during the entropy-driven structural optimization. Hence, an enthalpy-driven optimization process was preferred, by introducing a hydroxy group onto the C-3′-phenyl, as shown in a previous report.[15] In the present work, this strategy was extended to the design and synthesis of a series of more polar, high-affinity taxanes, including the representative **3f**.

Such taxanes (**3**), while leveraging the advantages against tumor drug resistance they could offer, are also more water-soluble than docetaxel (**1b**). It has been known[29] that the ease of formulation and lack of hypersensitive adverse effect of **1b** on injection (vs **1a**) can be attributed to the slightly improved aqueous solubility of **1b** relative to **1a**. Thus, it may be expected that taxane **3f** with both favored properties might exhibit better



DOI: 10.1021/acs.jnatprod.7b00857
J. Nat. Prod. XXXX, XXX, XXX−XXX

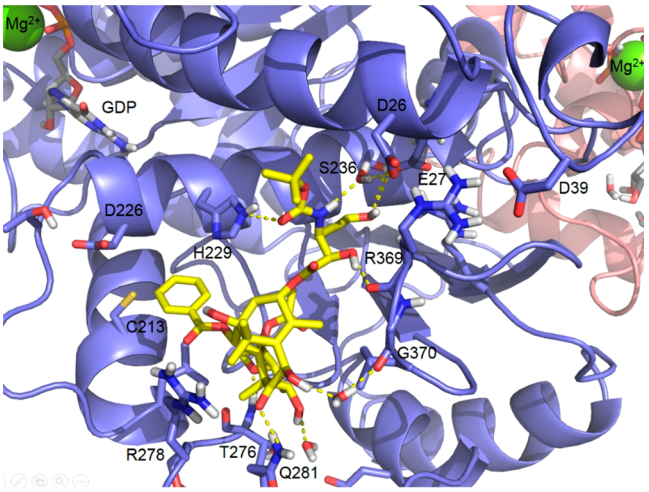


**Figure 3.** Close-up view of a representative snapshot from the molecular-dynamics (MD) trajectory showing **3f** (yellow sticks) bound at the interprotofilament taxane-binding site of $\beta$-tubulin (blue cartoon). Relevant protein residues are labeled and shown as sticks. Intermolecular hydrogen bonds are displayed as dashed yellow lines.

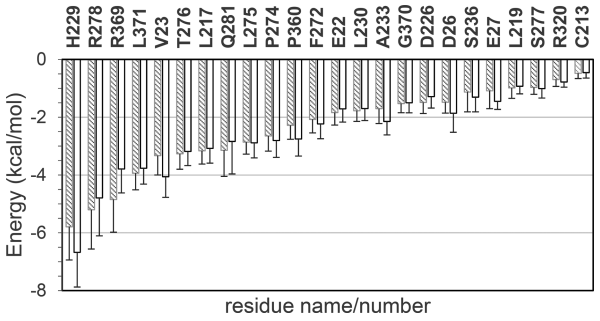


**Figure 4.** Calculated solvent-corrected interaction energies (kcal·mol$^{-1}$) between individual $\beta$-tubulin residues and either **3f** (hatched bars) or docetaxel (empty bars) bound at the interprotofilament site. For clarity, only the contributions achieving $\leq$1 kcal·mol$^{-1}$ are shown, which together represent a "binding fingerprint".

antitumor activity, especially against drug-resistant tumors. In xenograft animal testing, the antitumor effect of **3f** was comparable to those of the reference taxanes in drug-sensitive A2780 and much better in drug-resistant A2780AD xenografts. Such superior in vivo activity may be explained by not only slightly improved tubulin binding and thus cytotoxicity but also enhanced drug exposure (larger AUC and Cmax, Table S3, Supporting Information) and prolonged elimination (lower clearance, Table S3, Supporting Information) in animal models.

To assess the drug-like properties across the semisynthetic taxane family, the logP and ligand efficiency (LE) for commercial drugs **1a** and **1b**, hydrophobic taxanes **1e** and **1f** investigated as drug candidates, and two high-affinity taxanes (**2a** and **3f**) from this study were calculated. It was found that the LEs are comparable for all compounds, and the much higher clogPs for analogues **1e** and **1f** relative to marketed drugs may be related to their poor drug-like properties. In contrast, the lower clogP value for taxane **3f** is suggestive of an improved pharmaceutical profile (Table S4, Supporting Information).

In summary, enthalpy-driven optimization led to the discovery of semisynthetic taxanes inclusive of **3f**, which demonstrated improved pharmaceutical properties over commercially used taxane and thus the potential to be an antitumor drug.

## EXPERIMENTAL SECTION

**General Experimental Procedures.** $^1$H and $^{13}$C NMR spectra were recorded on Varian 300, 400, and 500 MHz NMR spectrometers or a Bruker AVANCE III 600 MHz NMR spectrometer. Mass spectra (ESI) were measured on a JEOL Accu TOF CS (JMS T100CS). Reagents were purchased from J&K and Alfa Aesar Chemical Companies. All anhydrous solvents were purified and dried according to standard procedures, unless otherwise indicated. Reactions were monitored by TLC (silica gel, GF254) with UV light and $H_2SO_4$-anisaldehyde spray visualization. The purity of the final taxoids was analyzed by HPLC.

The general procedure for the synthesis of compounds **2**, **3**, **5**−**13**, **15**−**22**, **24**, **25**, **27**, and **29**−**35** is provided in the Supporting Information, where full details of their purification and spectroscopic data are provided. Such information is given for compound **3f** below with the procedure for the biological testing and molecular modeling.

*3′-Dephenyl-3′-(3-hydroxyprop-1-ynyl)docetaxel (**3f**).* To a stirred solution of **15** (25 mg, 0.0323 mmol) in anhydrous tetrahydrofuran (THF) (0.42 mL) under argon and cooled to −45 °C was added dropwise lithium hexamethyldisilamide (LHMDS) (1.0 M in THF/ethylbenzene, 48.5 $\mu$L, 0.048 mmol). The reaction mixture was stirred for 20 min at −45 °C, and then the solution of **35b** (18 mg, 0.039 mmol) in anhydrous THF (0.1 mL) was added dropwise, the reaction mixture was stirred for 80 min at the same temperature, and LHMDS (1.0 M in THF/ethylbenzene, 48.5 $\mu$L, 0.048 mmol) was added dropwise. The reaction mixture was stirred for a further 1 h and then quenched with saturated aqueous $NH_4Cl$ solution (10 mL) and extracted with ethyl acetate (20 mL). The organic layer was washed with saturated aqueous $NH_4Cl$ solution (10 mL) and brine (10 mL) and dried over $Na_2SO_4$, and solvent was removed under reduced pressure to obtain the crude product without any further purification. Then, to a stirred solution of the crude product in acetonitrile (1.4 mL) was added Py/HF (2:1, 1.3 mL, 9.69 mmol), and the reaction mixture was stirred at room temperature for 24 h. Next, the mixture was diluted with ethyl acetate (20 mL), washed with saturated aqueous $NaHCO_3$ solution (10 mL) and brine (10 mL), and dried over anhydrous $Na_2SO_4$. The organic layer was evaporated under reduced pressure. Purification of the crude product by silica gel chromatography ($MeOH/CH_2Cl_2$, 1:25) gave 53% yield of **3f** as a colorless oil: $^1$H NMR ($CDCl_3$, 500 MHz) $\delta$ 8.10 (2H, d, $J$ = 7.5 Hz, Ar), 7.61 (1H, t, $J$ = 7.0 Hz, Ar), 7.50 (2H, t, $J$ = 8.0 Hz, Ar), 6.21 (1H, t, $J$ = 8.5 Hz, H-13), 5.67 (1H, d, $J$ = 6.5 Hz, H-2), 5.36 (1H, d, $J$ = 6.5 Hz, H-3′), 5.25 (1H, s, H-10), 4.99−4.95 (2H, m, H-5, N*H*), 4.44 (1H, s, H-2′), 4.33−4.18 (5H, m, H-20, H-7, C*H*$_2$), 3.91 (1H, d, $J$ = 7.0 Hz, H-3), 2.63−2.55 (1H, m, H-6a), 2.41 (3H, s, OAc), 2.32−2.25 (2H, m, H-14), 1.95 (3H, s, C*H*$_3$), 1.89−1.84 (1H, m, H-6b), 1.76 (3H, s, C*H*$_3$),

**Table 2. Binding Energies (kcal·mol$^{-1}$)[a] and Component Contributions[26] for the Association of 3f and Docetaxel with $\beta$-Tubulin at the Interprotofilament Site**

| complex | total | van der Waal's | coulombic | ligand desolvation | receptor desolvation | apolar |
|---|---|---|---|---|---|---|
| **3f** | −65.3 ± 4.5 | −66.0 ± 3.4 | −8.6 ± 1.9 | 4.9 ± 0.8 | 10.2 ± 2.5 | −5.8 ± 0.2 |
| docetaxel (**1b**) | −67.4 ± 5.9 | −70.6 ± 3.7 | −7.1 ± 1.7 | 4.6 ± 0.7 | 11.6 ± 2.7 | −6.0 ± 0.2 |

[a]Mean values and standard deviations calculated from 250 snapshots taken from the MD trajectories (25 ns).



DOI: 10.1021/acs.jnatprod.7b00857
J. Nat. Prod. XXXX, XXX, XXX−XXX

Table 3. Microtubule Binding Constants and Cytotoxicities of Taxanes 3 and Reference Drugs

| | | $IC_{50}$ (nM) | | | | | |
|---|---|---|---|---|---|---|---|
| compound | $K_b$ 35 °C ($M^{-1}$) | A2780 | A2780AD[a] | R/S[b] | HeLa | HeLa/βIII[c] | R/S[d] |
| paclitaxel (**1a**) | $3.3 \times 10^6$ | 13.4 | 16 040 | 1197 | 4.6 | 41.0 | 8.9 |
| docetaxel (**1b**) | $2.1 \times 10^7$ | 11.2 | 21 650 | 1933 | 3.5 | 27.1 | 7.7 |
| **3a** | $6.2 \times 10^6$ | 24.3 | 26 000 | 1070 | 28.8 | 612.5 | 21.3 |
| **3b** | $3.5 \times 10^5$ | 90.6 | 24 680 | 272 | 134.1 | 720.0 | 5.4 |
| **3c** | $<2 \times 10^4$ | 8934 | 15 650 | 1.8 | 14 140 | 3077 | 0.2 |
| **3d** | $<2 \times 10^4$ | >10 000 | ND | ND | 3527 | 25 050 | 7.1 |
| **3e** | $3.5 \times 10^5$ | 1926 | 18 830 | 9.8 | 2356 | 7961 | 3.4 |
| **3f** | $1.8 \times 10^8$ | 25.8 | 18 770 | 728 | 32.2 | 191.6 | 6.0 |
| **3g** | $3.5 \times 10^5$ | 462.7 | 20 630 | 44.6 | 707.3 | 1466 | 2.1 |
| **3h** | $5.1 \times 10^7$ | 73.8 | 25 310 | 343 | 53.3 | 404.6 | 7.6 |
| **3i** | $9.8 \times 10^6$ | 75.8 | 21 250 | 280 | 104.4 | 809.0 | 7.7 |

[a]Resistant ovarian carcinoma cells overexpressing P-gp. [b]The relative resistance values were calculated by dividing the $IC_{50}$ value of the resistant ovarian carcinoma cells by the $IC_{50}$ value of the nonresistant ovarian carcinoma cells. [c]βIII transfected human cervical carcinoma cells HeLa cell line (wild-type βIII). [d]The relative resistance values were calculated by dividing the $IC_{50}$ value of the βIII transfected cell line (wild-type βIII) by the $IC_{50}$ value of the parental HeLa cell line.

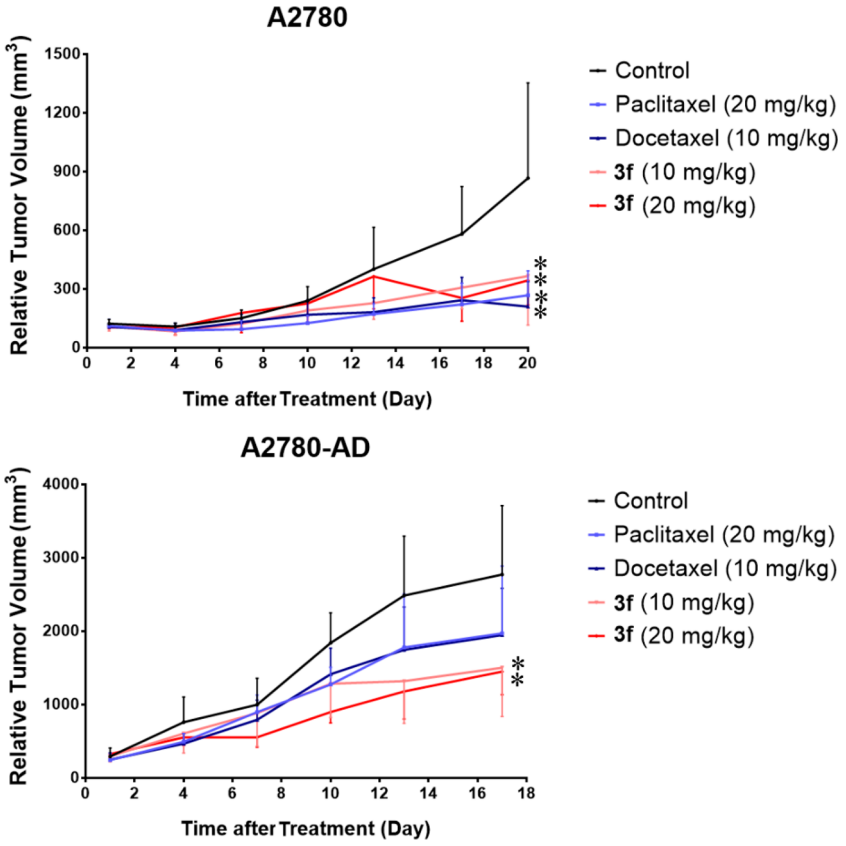


Figure 5. Inhibitory effects of **3f** on the tumor growth of A2780 and A2780AD in nude mice.

1.36 (9H, s, *t*-BuO), 1.21 (3H, s, $CH_3$), 1.13 (3H, s, $CH_3$); $^{13}C$ NMR ($CDCl_3$, 150 MHz) δ 211.2, 171.2, 170.6, 167.0, 154.9, 138.4, 136.0, 133.7, 130.1, 129.1, 128.7, 84.1, 83.1, 81.4, 81.1, 78.8, 76.6, 74.8, 74.6, 72.4, 72.0, 60.4, 57.7, 46.6, 43.1, 37.0, 35.6, 28.2, 26.4, 22.5, 20.5, 14.2, 9.9; ESIMS *m*/*z* 786.3 $[M + H]^+$, 808.3 $[M + Na]^+$.

**In Silico Model Building, Molecular Simulations and Binding Energy Analysis.** The simulated macromolecular ensemble representing a short piece of a microtubule with bound docetaxel (DXL, **1b**) and **3f** was built as previously reported for dictyostatin.[30] Briefly, (i) α-subunits A, E, I, and K and β-subunits B and F were selected from the cryo-electron microscopy reconstructions (PDB code 3J6G) of kinesin-decorated MTs in complex with paclitaxel solved at ∼5 Å resolution;[31] (ii) missing residues 39−48 in the four α-subunits, together with the partially hydrated $Ca^{2+}$ ion coordinated by Asp39, Thr41, Gly44, and Glu55 were added; (iii) the two guanosine diphosphate (GDP) and four guanosine triphosphate (GTP) molecules were present in the nucleotide-binding sites; and (iv) the docked poses of DXL and CTX-63 within the taxane-binding site in an α,β-tubulin dimer reported previously[15] were used to produce two different complexes in which DXL and **3f** occupied either the interprotofilament or the solvent-exposed site in two GDP and four GTP molecules' formation could be separately assessed.

Geometry optimization of DXL and **3f** was achieved by means of the updated AM1 Hamiltonian,[32] as implemented in the *sqm* program,[33] which also produced the atomic charge distributions for both ligands. The addition of missing hydrogen atoms to the protein


DOI: 10.1021/acs.jnatprod.7b00857
J. Nat. Prod. XXXX, XXX, XXX−XXX

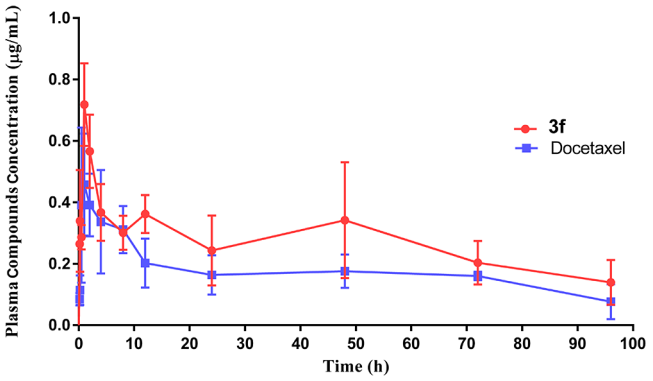


**Figure 6.** Docetaxel and **3f** plasma concentration−time profile in SD rats following a single ip dose at 10 mg/kg. Data are expressed as mean ± SD ($n$ = 3).

**Table 4. Water Solubility of Taxanes 2 and 3**

| compound | water solubility[a] (mg/mL) | fold | compound | water solubility (mg/mL) | fold |
|---|---|---|---|---|---|
| paclitaxel (**1a**) | 0.0003 | 1 | **3a** | 0.0093 | 31 |
| docetaxel (**1b**) | 0.006−0.007[b] | 20−23 | **3b** | 0.0143 | 48 |
| **2a** | 0.0126 | 42 | **3c** | 0.0406 | 135 |
| **2b** | 0.0109 | 36 | **3d** | 0.0244 | 81 |
| **2c** | 0.0111 | 37 | **3e** | 0.0289 | 96 |
| **2d** | 0.0125 | 42 | **3f** | 0.0192 | 64 |
| **2e** | 0.0149 | 50 | **3g** | 0.0186 | 62 |
| **2f** | 0.0112 | 37 | **3h** | 0.0137 | 46 |
| **2g** | 0.0095 | 32 | **3i** | 0.0274 | 91 |

[a]Water solubility was determined by reversed-phase HPLC at 25 °C. [b]Data from ref 28.

ensemble and computation of the protonation state of titratable groups at pH 6.5 were carried out using the H++ 3.0 Web server.[34] The ff14SB force field parameter set[35] in AMBER 14[36] was used to assign bonded and nonbonded parameters to protein and ligand atoms. Each complex was immersed in a cubic box containing ∼110 000 TIP3P water molecules plus >100 $Na^+$ ions to achieve electroneutrality and was simulated under periodic boundary conditions in the absence of any external restraints for 50 ns at 300 K. Electrostatic interactions were treated using the smooth particle mesh Ewald method[37] with a grid spacing of 1 Å. The cutoff distance for the nonbonded interactions was 9 Å, and the SHAKE algorithm[38] was applied to all bonds involving hydrogens so as to allow an integration step of 2.0 fs to be used. Subsequent gradual cooling, from 300 K to 273 K over 1 ns, of snapshots taken regularly every 2.5 ns, followed by energy minimization until the root-mean-square of the Cartesian elements of the gradient was less than 0.1 kcal·$mol^{-1}$·$Å^{-1}$, provided representative structures for the complexes. These sets of optimized coordinates were analyzed using the *cpptraj* routines implemented in the AmberTools14 suite[39] and the in-house MM-ISMSA software,[26] which provided the solvent-corrected binding energies as well as their decomposition into van der Waal's, Coulombic, apolar, and desolvation contributions.

**Binding Affinity Measurement.** Calf brain tubulin was purified as described.[40] Glutaraldehyde-stabilized microtubules with active paclitaxel binding sites were prepared as described.[41] The binding constants of the compounds to these microtubules were measured as previously described.[42]

**Cell-Based Assays.** Cytotoxicity evaluation was performed with A2780, A2780AD, (overexpressing P-gp),[43] human ovarian carcinoma cell lines, HeLa, and HeLa-$\beta$III transfected cells[44] with the MTT assay modified as previously described.[14] Cell cycle analysis was performed as previously described.[45]

**Preparation of Liposome 3f.** Liposomes **3f** were prepared using a film dispersion method following the published protocol.[46] Briefly, **3f**, lecithin, and cholesterol were dissolved initially in chloroform, and then the organic solvent was evaporated to obtain a membrane after 5 min of stirring. The resulting membrane was dissolved by the addition of phosphate-buffered saline to obtain a liposome solution. The solution obtained using this process was disrupted in an ultrasonic homogenizer. Then, the remaining solution was lyophilized to dried 19c liposomes using a freeze-dryer system (Labconco), and their microstructure was observed using a scanning electron microscope. Particle size was evaluated by means of a particle size analyzer (Mastersizer 2000, Malvern Instruments), and the encapsulation efficacy was measured using high-performance liquid chromatography (HPLC; Shimadzu LC-20A, $C_{18}$ column).

**Xenograft Studies.** Nude mice (6−8 weeks old, BALB/c, female) were used to establish the xenograft tumors following the published protocol.[47] Briefly, A2780/AD cells ($1 \times 10^7$) or A2780 cells ($5 \times 10^6$) were implanted in the dorsal region of recipient mice by means of subcutaneous injection. Once a tumor had reached around 300 $mm^3$ in size, the mice were randomized into five groups as control, paclitaxel (20 mg/kg), docetaxel (10 mg/kg), **3f**-low (10 mg/kg), and **3f**-high (20 mg/kg) with six or seven mice per group. The animals were administrated by intraperitoneal injection twice a week. Tumor growth and body weight were measured every three days during the treatment. At the end of the treatment, mice were sacrificed and tumors were removed and weighed. The use of animals was approved by the Animal Experimentation Ethics Committee of Yantai University (protocol number 20170605) in accordance with the guidelines for ethical conduct in the care and use of animals.

**Pharmacokinetic Experiments.** The pharmacokinetic profile of the **3f** in liposomes and Taxotere (docetaxel injection) were explored using SD rats (protocol number 20170711), after a single intraperitoneal injection at a dose of 10 mg/kg. Blood samples of about 500 $\mu$L were collected via the posterior orbit into a heparinized vacutainer tube at 0, 0.17, 0.25, 0.5, 1, 2, 4, 8, 12, 24, 48, 72, and 96 h postadministration. The blood samples were centrifuged at 4000 rpm for 10 min at 4 °C to obtain plasma samples, which were kept frozen at −80 °C until analysis. Each plasma sample (50 $\mu$L) was treated with 200 $\mu$L of acetonitrile and vortexed for 30 s followed by centrifugation at 12 000 rpm for 10 min at 4 °C. Then, the supernatants were transferred to other test tubes. The **3f** concentration in the plasma samples was quantified using a Diamonsil C18 (4.6 mm × 6250 mm; ⌀ 5 mm) HPLC column at a temperature of 30 °C. The mobile phase was 55:45 (acetonitrile/water) for **3f** and 70:30 (acetonitrile/water) for docetaxel at a flow rate of 1 mL/min. The effluent was detected at 230 nm, and the area under the peak was used for quantification. Pharmacokinetic parameters were calculated using the noncompartmental analysis with DAS 2.0 (Drug and Statistics) Software.

**Partition Coefficient (LogP Value) Calculations.** CLogP value calculations were performed with ChemBioDraw Ultra 11.0 and Accelrys Discovery Studio 2.5. Structures of ligands were drawn using ChemBioDraw Ultra 11.0 and saved as sdf file. The sdf file was opened by Accelrys Discovery Studio 2.5, and cLogP values were calculated by Protocols-General Purpose-Calculate Molecular Properties as "ALogP" in the software. The results are shown in Table S4, Supporting Information.

## ■ ASSOCIATED CONTENT

### Supporting Information

The Supporting Information is available free of charge on the ACS Publications website at DOI: 10.1021/acs.jnatprod.7b00857.

Addtional information (PDF)

Spectra (PDF)



DOI: 10.1021/acs.jnatprod.7b00857
J. Nat. Prod. XXXX, XXX, XXX−XXX

## AUTHOR INFORMATION


### Corresponding Authors

*Tel: +86 138 5357 9172. E-mail: hongbowangyt@gmail.com (H. Wang).

*Tel: +86 010-63165229. Fax: +86 010-63017757. E-mail: wfang@imm.ac.cn (W.-S. Fang).

### ORCID

Yun-Tao Ma: 0000-0002-8961-9445

Federico Gago: 0000-0002-3071-4878


### Notes

The authors declare no competing financial interest.

## ACKNOWLEDGMENTS

The authors acknowledge the financial support by NSFC (grant no. 30930108), CIFMS (grant no. 2016-I2M-1-010), and the Spanish MINECO (grant no. SAF2015-64629-C2-2-R).

## DEDICATION

Dedicated to Dr. Susan Band Horwitz, of Albert Einstein College of Medicine, Bronx, NY, for her pioneering work on bioactive natural products.

## REFERENCES


(1) http://www.who.int/mediacentre/factsheets/fs297/en/.

(2) Yang, C.-P. H.; Horwitz, S. B. *Int. J. Mol. Sci.* **2017**, *18*, 1733−1743.

(3) Ozols, R. F. *Semin. Oncol.* **1994**, *21*, 1−9.

(4) Seidman, A. D.; Reichman, B. S.; Crown, J. P.; Yao, T. J.; Currie, V.; Hakes, T. B.; Hudis, C. A.; Gilewski, T. A.; Baselga, J.; Forsythe, P.; Lepore, J.; Marks, L.; Fain, K.; Souhrada, M.; Onetto, N.; Arbuck, S.; Norton, L. *J. Clin. Oncol.* **1995**, *13*, 1152−1159.

(5) Ojima, I.; Lichtenthal, B.; Lee, S.; Wang, C.-W.; Wang, X. *Expert Opin. Ther. Pat.* **2016**, *26*, 1−20.

(6) Singla, A. K.; Garg, A.; Aggarwal, D. *Int. J. Pharm.* **2002**, *235*, 179−192.

(7) Casazza, A. M.; Fairchild, C. R. In *Drug Resistance*; Hait, W. N., Ed.; Kluwer Academic Publishers: Boston, 1996; Vol. *87*, Chapter 6, pp 149−171.

(8) Murray, S.; Briasoulis, E.; Linardou, H.; Bafaloukos, D.; Papadimitriou, C. *Cancer Treat. Rev.* **2012**, *38*, 890−903.

(9) Orr, G. A.; Verdier-Pinard, P.; McDaid, H.; Horwitz, S. B. *Oncogene* **2003**, *22*, 7280−7295.

(10) Ferlini, C.; Gallo, D.; Scambia, G. *Expert Opin. Invest. Drugs* **2008**, *17*, 335−347.

(11) Matesanz, R.; Trigili, C.; Rodriguez-Salarichs, J.; Zanardi, I.; Pera, B.; Nogales, A.; Fang, W. S.; Jimenez-Barbero, J.; Canales, A.; Barasoain, I.; Ojima, I.; Diaz, J. F. *Bioorg. Med. Chem.* **2014**, *22*, 5078−5090.

(12) Mita, A. C.; Denis, L. J.; Rowinsky, E. K.; DeBono, J. S.; Goetz, A. D.; Ochoa, L.; Forouzesh, B.; Beeram, M.; Patnaik, A.; Molpus, K.; Semiond, D.; Besenval, M.; Tolcher, A. W. *Clin. Cancer Res.* **2009**, *15*, 723−730.

(13) U.S. FDA Center for Drug Evaluation and Research. Approval Package for Jevtana. June 17, 2010. Available from https://www.accessdata.fda.gov/drugsatfda_docs/nda/2010/201023s000Approv.pdf.

(14) Yang, C.-G.; Barasoain, I.; Li, X.; Matesanz, R.; Liu, R.-H.; Sharom, F. J.; Yin, D. L.; Diaz, J. F.; Fang, W.-S. *ChemMedChem* **2007**, *2*, 691−701.

(15) Coderch, C.; Tang, Y.; Klett, J.; Zhang, S. E.; Ma, Y. T.; Wang, S. R.; Matesanz, R.; Pera, B.; Canales, A.; Jimenez-Barbero, J.; Morreale, A.; Diaz, J. F.; Fang, W. S.; Gago, F. *Org. Biomol. Chem.* **2013**, *11*, 3046−3056.

(16) Zhou, Q.; Li, Y.; Jin, J.; Lang, L.-W.; Zhu, Z.-X.; Fang, W.-S.; Chen, X.-G. *Biol. Pharm. Bull.* **2012**, *35*, 2170−2179.

(17) Matesanz, R.; Barasoain, I.; Yang, C.-G.; Wang, L.; Li, X.; Ines, C.; Coderch, C.; Gago, F.; Jimenez-Barbero, J.; Andreu, J. M.; Fang, W. S.; Diaz, J. F. *Chem. Biol.* **2008**, *15*, 573−585.

(18) Cai, P.; Lu, P.-H.; Sharom, F. J.; Fang, W.-S. *Cancer Lett.* **2013**, *341*, 214−223.

(19) Meanwell, N. A. *Chem. Res. Toxicol.* **2011**, *24*, 1420−1456.

(20) Hann, M. M. *MedChemComm* **2011**, *2*, 349−355.

(21) Ojima, I.; Slater, J. C.; Michaud, E.; Kuduk, S. D.; Bounaud, P.-Y.; Vrignaud, P.; Bissery, M.-C.; Veith, J. M.; Pera, P.; Bernacki, R. J. *J. Med. Chem.* **1996**, *39*, 3889−3896.

(22) Tang, Y.; Rodriguez-Salarichs, J.; Zhao, Y.; Cai, P.; Estevez-Gallego, J.; Balaguer-Perez, F.; Horcajo, M. R.; Lucena-Agell, D.; Barasoain, I.; Diaz, J. F.; Fang, W.-S. *Eur. J. Med. Chem.* **2017**, *137*, 488−503.

(23) Kingston, D. G. I.; Chaudhary, A. G.; Chordia, M. D.; Gharpure, M.; Gunatilaka, A. A. L.; Higgs, P. I.; Rimoldi, J. M.; Samala, L.; Jagtap, P. G. *J. Med. Chem.* **1998**, *41*, 3715−3726.

(24) Kingston, D. G. I.; Newman, D. J. *Curr. Opin. Drug Discovery Dev.* **2007**, *10*, 130−144.

(25) Cramer, J.; Krimmer, S. G.; Heine, A.; Klebe, G. *J. Med. Chem.* **2017**, *60*, 5791−5799.

(26) Klett, J.; Núñez-Salgado, A.; Dos Santos, H. G.; Cortés-Cabrera, Á.; Perona, A.; Gil-Redondo, R.; Abia, D.; Gago, F.; Morreale, A. *J. Chem. Theory Comput.* **2012**, *8*, 3395−3408.

(27) Ali, S. M.; Hoemann, M. Z.; Aube, J.; Mitscher, L. A.; Georg, G. I. *J. Med. Chem.* **1995**, *38*, 3821−3828.

(28) Du, W.; Hong, L.; Yao, T.; Yang, X.; He, Q.; Yang, B.; Hu, Y. *Bioorg. Med. Chem.* **2007**, *15*, 6323−6330.

(29) Hennenfent, K. L.; Govindan, R. *Ann. Oncol.* **2006**, *17*, 735−749.

(30) Trigili, C.; Barasoain, I.; Sánchez-Murcia, P. A.; Bargsten, K.; Redondo-Horcajo, M.; Nogales, A.; Gardner, N. M.; Meyer, A.; Naylor, G. J.; Gómez-Rubio, E.; Gago, F.; Steinmetz, M. O.; Paterson, I.; Prota, A. E.; Díaz, J. F. *ACS Omega* **2016**, *1*, 1192−1204.

(31) Alushin, G. M.; Lander, G. C.; Kellogg, E. H.; Zhang, R.; Baker, D.; Nogales, E. *Cell* **2014**, *157*, 1117−1129.

(32) Rocha, G. B.; Freire, R. O.; Simas, A. M.; Stewart, J. J. P. *J. Comput. Chem.* **2006**, *27*, 1101−1111.

(33) Walker, R. C.; Crowley, M. F.; Case, D. A. *J. Comput. Chem.* **2008**, *29*, 1019−1031.

(34) Anandakrishnan, R.; Aguilar, B.; Onufriev, A. V. *Nucleic Acids Res.* **2012**, *40*, W537−541.

(35) Maier, J. A.; Martinez, C.; Kasavajhala, K.; Wickstrom, L.; Hauser, K. E.; Simmerling, C. *J. Chem. Theory Comput.* **2015**, *11*, 3696−3713.

(36) Kaus, J. W.; Pierce, L. T.; Walker, R. C.; McCammon, J. A. *J. Chem. Theory Comput.* **2013**, *9*, 4131−4139.

(37) Cerutti, D. S.; Duke, R. E.; Darden, T. A.; Lybrand, T. P. *J. Chem. Theory Comput.* **2009**, *5*, 2322−2338.

(38) Ryckaert, J.-P.; Ciccotti, G.; Berendsen, H. J. C. *J. Comput. Phys.* **1977**, *23*, 327−341.

(39) Case, D. A.; Berryman, J. T.; Betz, R. M.; Cerutti, D. S.; Cheatham, T. E., III; Darden, T. A.; Duke, R. E.; Giese, T. J.; Gohlke, H.; Goetz, A. W.; Homeyer, N.; Izadi, S.; Janowski, P.; Kaus, J.; Kovalenko, A.; Lee, T. S.; LeGrand, S.; Li, P.; Luchko, T.; Luo, R.; Madej, B.; Merz, K. M.; Monard, G.; Needham, P.; Nguyen, H.; Nguyen, H. T.; Omelyan, I.; Onufriev, A.; Roe, D. R.; Roitberg, A.; Salomon-Ferrer, R.; Simmerling, C. L.; Smith, W.; Swails, J.; Walker, R. C.; Wang, J.; Wolf, R. M.; Wu, X.; York, D. M.; Kollman, P. A. *AMBER 2015*, San Francisco, 2015.

(40) Andreu, J. M. In *Microtubule Protocols, Methods in Molecular Medicine*; Zhou, J., Ed.; Humana Press: Totowa, NJ, 2007; Vol. *137*, Chapter 2, pp 17−28.

(41) Díaz, J. F.; Barasoain, I.; Andreu, J. M. *J. Biol. Chem.* **2003**, *278*, 8407−8419.

(42) Buey, R. M.; Díaz, J. F.; Andreu, J. M.; O'Brate, A.; Giannakakou, P.; Nicolaou, K. C.; Sasmal, P. K.; Ritzén, A.; Namoto, K. *Chem. Biol.* **2004**, *11*, 225−236.




DOI: 10.1021/acs.jnatprod.7b00857
*J. Nat. Prod.* XXXX, XXX, XXX−XXX

(43) Kowalski, R. J.; Giannakakou, P.; Gunasekera, S. P.; Longley, R. E.; Day, B. W.; Hamel, E. *Mol. Pharmacol.* **1997**, *52*, 613−622.
(44) Joe, P. A.; Banerjee, A.; Ludueña, R. F. *Cell Motil. Cytoskeleton* **2008**, *65*, 476−486.
(45) Lowe, J.; Li, H.; Downing, K. H.; Nogales, E. *J. Mol. Biol.* **2001**, *313*, 1045−1057.
(46) Wang, H. B.; Zhang, J. Q.; Lv, G. Y.; Ma, J. B.; Ma, P. K.; Du, G. Y.; Wang, Z. L.; Tian, J. W.; Fang, W. S.; Fu, F. H. *PLoS One* **2014**, *9*, e114688.
(47) Wang, H. B.; Li, H. Y.; Zuo, M. X.; Zhang, Y.; Liu, H.; Fang, W. S.; Chen, X. G. *Cancer Lett.* **2008**, *268*, 89−97.



DOI: 10.1021/acs.jnatprod.7b00857
*J. Nat. Prod.* XXXX, XXX, XXX−XXX